N–hydroxybenzothioamide derivatives as green and efficient corrosion inhibitors for mild steel: Experimental, DFT and MC simulation approach

Dakeshwar Kumar Verma [a,*], Mohsin Kazi [b], Mohammed S. Alqahtani [b], Rabbani Syed [b], Elyor Berdimurodov [c,*], Savaş Kaya [d], Rajae Salim [e], Ashish Asatkar [f], Rajesh Haldhar [g]

[a] Department of Chemistry, Government Digvijay Autonomous Postgraduate College, Rajnandgaon, Chhattisgarh, INDIA, 491441
[b] Department of Pharmaceutics, College of Pharmacy, PO Box 2457, King Saud University, Riyadh, 11451, Saudi Arabia
[c] Faculty of Natural Sciences, Karshi State University, Karshi, 180100, Uzbekistan
[d] Cumhuriyet University Health Services Vocational School, Department of Pharmacy, 58140 Sivas, Turkey
[e] Laboratory of Engineering, organometallic, Molecular and Environment (LIMOME), Faculty of science, University Sidi Mohamed Ben Abdellah, Fez, Morocco
[f] Department of Chemistry, Govt. Gundadhur Postgraduate College, Kondagaon, Chhattisgarh, INDIA
[g] School of Chemical Engineering, Yeungnam University, Gyeongsan 712749, SOUTH KOREA

ARTICLE INFO

ABSTRACT

In this research work, the thiohydroxamic acid derivatives included N–hydroxybenzothioamide (THA–H), 4–bromo–N–hydroxybenzothioamide (THA–Br), and 4–methoxy–N–hydroxybenzothioamide (THA–OCH$_3$) were first introduced as effective and green corrosion inhibitors for mild steel in 1M HCl. The inhibition behaviours of THA–H, THA–Br and THA–OCH$_3$ were first–fully characterized by weight loss (WL), potentiodynamic polarization (PDP), and electrochemical impedance spectroscopy (EIS). The obtained experimental results suggested that the maximum inhibition efficiency of THA–H, THA–Br and THA–OCH$_3$ were over 90% at 300 ppm. The surface characterization of the metal surface was investigated by X–ray diffraction analysis (XRD), scanning electron microscope (SEM) and electron diffraction X–ray spectroscopy (EDS) analysis; the obtained results confirmed that the selected inhibitors formed the protective film on the metal surface. The quantum chemical analysis and Monte Carlo (MC) simulation were also performed to determine the nature of adsorption, possible adsorption orientation of inhibitor molecules on the metal surface, the correlation between the inhibition properties and molecular structures. Adsorption isotherm suggests that the selected molecules are mixed type of corrosion inhibitors related to Langmuir isotherm.

1. Introduction

Mild steel is a widely used metallic material in the gas and oil industry. The corrosion of metallic materials is a large problem environmentally and economically [1]. The metal surface was destroyed by the corrosion processes. As a result, the mechanical properties of metal was dramatically reduced [1-3]. For example, the metal pipes were made from mild steel in the gas and oil industry. The metal pipes were seriously corroded during oil and gas transportation. Consequently, the surface of steel pipes was covered with corrosion deposits such as salts, hydroxide and oxides [4]. The corrosion deposits inside metal pipes are difficult for gas and oil transportation [5]. To clean the corrosion products from the metal surface, 1 M HCl was used. The metal surface was corroded during the cleaning processes. This is due to the acidic attacks on the surface of the metal. Protecting the metal pipes from the corrosion processes is an important task in the gas and oil industry [6]. The corrosion inhibitor was added to the corrosion solution to protect the metal surface from corrosion destruction. In the inhibition processes, the corrosion inhibitor adsorbed on the metal surface to form the protective film [7]. As a consequence, the metal surface was protected and corrosion deposits were reduced. The corrosion inhibitors are organic compounds, which have more heteroatoms,

functional groups and benzoyl rings [8]. Generally, the corrosion inhibitors contained nitrogen, sulfur, oxygen and phosphorous, and aromatic rings. They are mainly responsible for corrosion protection [9]. The corrosion inhibitor chemical and physical adsorbed on the metal surface by the heteroatoms, functional groups and benzoyl rings [10].

It was known that the p–electron containing organic molecules are excellent corrosion inhibitors because the p–electrons in the corrosion inhibitor interact easily with the empty d–orbitals of metal to form a stable complex on the metal surface;as a result, the metallic surface is protected from the corrosive attack [4-9].Currently, there several types of heterocyclic compounds were investigated as an efficient corrosion inhibitors. For example, the imidazole derivatives [10], porphyrin, hydrazide [11,12], hydroxamic acid derivatives [13,14], tetrazole derivatives [15] and porphines derivatives [16] were mostly used.

The novelty of this research work, the thiohydroxamic acid derivatives (THAs) included [(N–hydroxybenzothioamide (THA–H), 4–bromo-N–hydroxybenzothioamide (THA–Br), and 4–methoxy–N–hydroxybenzothioamide (THA–OCH$_3$)] were first introduced as effective corrosion inhibitors for mild steel in the 1M HCl corrosive solution. These derivatives contain the nitrogen, oxygen, and sulphur heteroatom as well as p–electron and aromatic ring, which support to become high inhibition efficiency of these inhibitors. Also, the thiohydroxamic acid derivatives have been used as an antioxidant and tyrosinase inhibitor [17], anticancer, antibacterial agents [18] and in extraction and speciation of Plutonium [19]. These properties support that the selected corrosion inhibitors are green and excellent. Additionally, THAs contain electron donor nitrogen and oxygen heteroatoms, which can promote form the stable complexes with iron metal ions on the metal surface. Also, THAs are good chelating ligands. This is due to their complexation behaviour with metal cation to form thermodynamically stable five-membered chelate complexes [20]. Their high complexation ability also supports the formation of a stable complex with iron ions and adsorb on the metal surface.Therefore, hydroxamic acid can be applied as a green alternative corrosion inhibitor with high inhibition efficiency at low concentrations. Recently, few research works suggested that hydroxamic acid is an efficient corrosion inhibitor for metals and alloys [14,21,22].Therefore,the hydroxamic acids and their derivatives can be considered as environmentally friendly alternatives to traditional toxic corrosion inhibitors. In addition to this, THA–H, THA–Br and THA–OCH$_3$ easily formed the complex with iron ions. These complex effectively adsorbed on the steel surface. The formed complex are not toxic. This is due to the active functional groups and heteroatoms in the THA–H, THA–Br and THA–OCH$_3$ are linked with the iron ions. As a result, all functional groups are blocked and toxic properties of THA–H, THA–Br and THA–OCH$_3$ dramatically reduced. In addition to this, the corrosion inhibitors rigid adsorbed on the steel surface and strongly linked with metal surface. Consequently, the toxic properties of THA–H, THA–Br and THA–OCH$_3$ are importantly reduced. Therefore, it was suggested that the THA–H, THA–Br and THA–OCH$_3$ are environmental-friendly and more efficient corrosion inhibitor for steel metallic material.Therefore, they have been used in current research as corrosion inhibitors for mild steel in an acidic medium (1M HCl). Modern experimental methods such as gravimetric analysis, electrochemical impendence spectroscopy (EIS), and potentiodynamic polarization (PDP) have been used for the characterization of inhibition efficiency and electrochemical behaviour. Surface analysis techniques such as X-ray diffraction analysis (XRD), scanning electron microscopy (SEM) and electron dispersion X–ray spectroscopy (EDS) have also been performed to identify the surface morphology. Theoretical calculations such as the density functional theory (DFT) and Monte Carlo (MC) simulation have been applied to describe the nature of adsorption, possible adsorption

orientation of inhibitor molecules on the metal surface, the correlation between the inhibition properties and molecular structures.

2. Methods and materials

2.1. Metal specimen and test solution

In this research work, the mild steel (MS) sample was purchased from the commercial company (Raipur, INDIA). It was a composite material that included the following elements: ~98%Fe, 0.3% Cu, 0.3% Ni, 0.3% Cr, 0.25–0.5% Mn, 0.05% S, 0.09–0.22% C, 0.05–0.15% Si, 0.008% N, 0.04% P and 0.08% As. These metal samples were applied for both electrochemical and mass loss measurements. Hydrochloric acid (36.5%) purchased from the commercial chemical company (MERCK grade, Raipur, INDIA)) and used to prepare the 1M HCl for corrosive medium, in which different amounts of inhibitors (150 to 300 ppm) were dissolved for the gravimetric and electrochemical measurements. In all experiments, the mild steel specimens should be were carefully scratched with different grades (200–1200) of emery papers to get a clean and smooth surface. After a scratch, the specimen was washed with double distilled and acetone for the removal of dust and grease. Then, the metal specimen was kept in the desiccators before use for a sufficient period (up to 15 minutes).

2.2. Synthesis of inhibitors

All chemicals were purchased from a commercial chemical company (MERCK grade, Raipur, INDIA). All chemical reactions were monitored by pre-coated silica gel 60 F$_{254}$ plates (250 mm layer thickness thin layer) chromatography (TLC) analysis. Melting points of all synthesised compounds were determined using a capillary melting point apparatus (METTELAR TOLEDEO, Germany).

The N–hydroxybenzothioamide (THA–H) was synthesized related to the following procedures: 2.00 g (12.9 mmol) N–hydroxybenzimidoyl chloride and 9.26 g (38.6 mmol) Na$_2$S were added in 172 mL (12.9 mmol) triethylamine solvent. Next, this mixture was stirred for one hour. After one hour, 5 M HCl was added to the formed mixture. As a result, the green solid crystal (THA–H) was formed. Finally, the THA–H crystal was separated using the separation funnel. The reaction yield of THA–H was 65%.
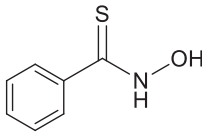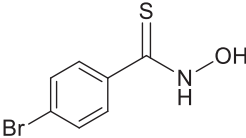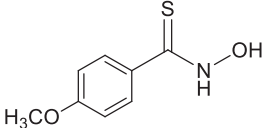
4–Bromo–N–hydroxybenzothioamide (THA–Br) was prepared according to the following procedures: 0.43 g (5.5 mmol) 4–bromo–N–hydroxybenzimidoyl chloride and 1.3 g (5.5 mmol) Na$_2$S were added in trimethylamine/water solvent system. The mixture was stirred for one hour to form a yellow solid crystal. Finally, the yellow crystal THA–Br was separated using the separation funnel. The reaction yield of THA–Br was 48%.

N–Hydroxy–4–methoxybenzothioamide (THA–OCH$_3$) was synthesized related tothe following steps: 0.10 g (0.54 mmol) N–hydroxy–4–methoxybenzimidoyl chloride, 0.39 g (1.6 mmol) Na$_2$S and 0.075 mL (0.54 mmol) trimethylamine were mixed and stirred for one hour. As a result, the solid yellow crystal of THA–OCH$_3$ was formed. Finally, the yellow crystal was obtained with a 52% reaction yield [23]. Additionally, Table 1 illustrates the structure, name, and analytical spectral data of THAs derivatives.

2.3. Weight loss analysis

2.5 × 1.0 × 0.1 cm^3 (H×W×T) mild steel specimens wereused in the present investigation, and all experimentswere carried out according to the standard procedure of ASTM G1 [24]. Weight loss measurement was applied atthe various concentration (200, 250 and 300 ppm) of inhibitorin 1M HCl with the different temperatures (from 298 K to 328 K). Before experimenting, the mild steel samples were dipped carefully in the electrolytic solution

Table 1

Structure, name and analytical spectral data of THAs derivatives

S.N.	IUPAC name	Structure	Analytical and spectral data
1	N-hydroxybenzothioamide	Molecular Weight: 153.20 **(THA-H)**	Mol. Formula: C_7H_7NOS Yield (65%); mp: 40 (±1)°C; 1H NMR (400 MHz) δ 7.2 (d, 1 H), 7.9 (d 1H), 10.2 (m, 5 H) IR (film); 3175, 1683.84, 1477.85, 1290.05, 1144.78 cm^{-1}
2	4-bromo-N-hydroxybenzothioamide	Molecular Weight: 232.10 **(THA-Br)**	Mol. Formula: C_7H_6BrNOS Yield (48%); mp: 108(±2)°C; 1H NMR (400 MHz) δ 6.2 (d, 1H), 6.6 (m, 2H), 7.0 (2H) IR (film); 3239.62, 3024.90, 1626.55, 1431.60, 1225 cm^{-1}
3	4-methoxy-N-hydroxybenzothioamide	Molecular Weight: 183.23 **(THA-OCH₃)**	Mol. Formula: $C_8H_9NO_2S$ Yield (52%); mp: 97 (±1)°C; 1H NMR (400 MHz) δ 3.8 (s, 2 H), 6.1 (d, 1 H), 7.1 (s, 2 H); 7.5 (s 2H), 9.2 (s 1H) IR (film); 3322.18, 1600.69, 1485.89, 1274.33, 1151.35 cm^{-1}

Table 2

Weight loss parameters of THAs derivatives.

Inhibitor	Conc. (ppm)	Corrosion Rate, ρ, (mg cm^{-2} h^{-1})				Inhibition Efficiency (%η)			
		298K	308K	318K	328K	298K	308K	318K	328K
THA-OCH₃	0.0	1.080	1.905	4.046	5.170	-	-	-	-
	150	0.188	0.346	0.755	1.396	82.59	81.83	81.34	73.00
	200	0.143	0.294	0.656	1.322	86.95	84.57	83.79	74.43
	250	0.095	0.251	0.601	1.101	91.21	86.82	85.14	78.70
	300	0.062	0.201	0.558	0.982	**94.26**	88.45	86.20	81.01
THA-H	0.0	1.135	2.166	4.160	5.372	-	-	-	-
	150	0.193	0.444	0.888	1.692	82.99	79.50	78.60	68.50
	200	0.151	0.374	0.773	1.574	86.69	82.73	81.41	70.70
	250	0.110	0.291	0.635	1.2961	90.30	86.56	84.738	75.87
	300	0.077	0.241	0.575	.102	**93.21**	88.87	86.17	79.48
THA-Br	0.0	1.280	2.311	4.313	5.520	-	-	-	-
	150	0.255	0.502	0.962	1.755	80.07	78.28	77.70	68.20
	200	0.209	0.432	0.841	1.643	83.67	81.30	80.52	70.26
	250	0.173	0.356	0.696	1.3651	86.48	84.59	83.868	75.28
	300	0.111	0.306	0.638	.170	**91.32**	86.75	85.20	78.80

and inhibited solutions for 6 hours. After 6h, the specimen was carefully taken out from the solutions and then the metal specimen was dried with distilled water and acetone. Finally, the dried metal sample was weighed three times with METALLER TOLEDO electronic equipment. To study the effect of temperature, the experiments were performedat different temperatures (298K –328K) in solutions with different concentrations. The obtained weight loss results are presented in Table 2. The corrosion rate (ρ) at mg/cm^2×hour was calculated from Eq. 1 [25]:

$$\rho = \frac{\Delta W}{At} \tag{1}$$

where, ΔW, A, and t represent the weight loss (mg/cm^2×hour), the metallic surface area (at cm^2), and time (6h), respectively.

The inhibition efficiency (%η) was calculated according to Eq. 2 [25]:

$$\%\eta_{WL} = \frac{w_o - w_i}{w_o} \times 100 \tag{2}$$

where, w_o and w_i represent the weight loss of mild steel sample in the corrosive and inhibited medium, respectively.

2.4. Electrochemical analysis

Echem analyst 5.0 (Gamy potentiostat software G–300) was used in current research to perform the electrochemical measurement [26]. Three–electrode sample was designed to do all electrochemical experiments at 298K temperature. Three–electrode sample contained SCE (reference electrode), mild steel (working electrode), and platinum (counter electrode). The bottom side of mild steel (1 cm^2) electrodes were dipped into the electrolytic solution, and the remaining parts of mild steelwere covered with the epoxy resin of adhesive Araldite. The potentiodynamic polarization (PDP) was recorded at the scan range 1m V s^{-1}and the potential range of $\pm$ 250 mV. It was used 1 mV/s polarization rate. This is due to this rate is standard in corrosion inhibition investigations. To use 1 mV/s polarization rate supports to obtain more accurate results in the polarization analysis.The inhibition performance was estimated

according to Eq. 3 [21]:

$$\%\eta_{PDP} = \frac{i^o_{corr} - i^i_{corr}}{i^o_{corr}} \times 100 \tag{3}$$

where, i^o_{corr} and i^i_{corr} represent the corrosion current densities in the inhibitor absence and presence solutions, respectively.

EIS analyses were applied from 100KHz to 0.01 MHz frequency range with an amplitude of −10 mV. Then, the Nyquist curves for the MS corrosion in 1M HCl solution were found with the best equivalent circuit model (Fig. 5), which consists of a constant phase (CPE) element or a charge transfer resistance (R_{ct}) and solution resistance (R_c).The inhibition efficiency ($\%\eta_{EIS}$) of inhibitor was calculated from the values of charge transfer resistance using Eq. 4 [21].

$$\%\eta_{EIS} = \frac{R^i_{ct} - R^o_{ct}}{R^i_{ct}} \times 100 \tag{4}$$

where, R^i_{ct} and R^o_{ct} represents the charge transfer resistance in the inhibited and uninhibited 1M HCl.

2.5. Surface analysis

SEM analysis was performed to analyse the surface morphology of the metal specimen while EDS was used to find the composition of the metal surface [27]. In the present work, the mild steel sample has been employed for surface analysis after 4h immersion time. In the surface analysis, the 300 ppm inhibitor was used. After an immersion time, the metal sample was taken out and washed three times with distilled water and acetone. Next, the dried metal sample was prepared for SEM–EDS analysis.1S kV accelerating voltage was performed to take the image with 500X magnification and the spectrum of SEM–EDS. XRD analysis is another advanced tool for surface characterization, which reveals the nature of the deposit protective layer on the metal surface. The specimens obtained from the weight loss measurement were scratched with a soft hand using a new knife. PAN analytical 3 KW–expert powder multifunction, Netherland X–ray diffractometer was used for XRD analysis applying CuKα radiation with an angular range of 60°> 2θ> 0° at 298K.

2.6. Quantum chemical calculation analysis

Quantum chemical calculations based on DFT were applied to identify the efficiency of organic molecules and observe the quantum chemical parameters, which are responsible for inhibition characteristics [28]. In the present investigation, Gaussian 09 software was employed for DFT calculation with optimized structures of inhibitors. Li–Yang–Cross non–local correlation function (B3L4P) and 21G based hybrid sets were applied to determine the electronic properties of the inhibitors:THA–H, THA–Brand THA–OCH$_3$.The electronic affinity and ionization energy were determined using the energy of Frontier molecular orbitals (HOMO and LUMO).Additionally, other important parameters such as the dipole moment, global hardness, energy gap, electronegativity and fraction of electron were also calculated from the Eqs. 5–10 [22]:

$$IE = -E_{HOMO} \tag{5}$$

$$EA = -E_{LUMO} \tag{6}$$

$$\eta = \frac{1}{2}(IE - EA) = \frac{1}{2}(-E_{HOMO} + E_{LUMO}) \tag{7}$$

$$\sigma = \frac{1}{\eta} \tag{8}$$

$$\chi = \frac{1}{2}(IE + EA) = \frac{1}{2}(-E_{HOMO} - E_{LUMO}) \tag{9}$$

$$\Delta N = \frac{\chi_{Fe} - \chi_{inh}}{2(\eta_{Fe} + \eta_{inh})} \tag{10}$$

where, the electronegativity was 4.88 eV for Fe has been applied for the calculation of electron transfer (ΔN).

2.7. Monte Carlo simulation analysis

The Monte Carlo simulation study is an interesting technique, which can provide us with more information about the interfacial interactions between the steel surface and studied inhibitors molecule [29].Therefore, the present investigation was conducted to study the interaction with the aqueous phase (200 H$_2$O, 5 H$_3$O$^+$, and 5 Cl$^-$), and a steel surface Fe(110) using the adsorption locator module in the Materials Studio 2017 software [30]. The most suitable stable adsorbed configuration of the studied molecule on the surface of Fe (110) is related to the higher negative adsorption energy values. All components of the simulation system were optimized via the Forcite module using the COMPASS force field [27].The Fe (110) crystal was built with a 30 Å edge to achieve enough depth then enlarged to create a supercell (12 × 12).

3. Results and discussions

3.1. Weight loss measurement: Effect of concentrations

It is clear from the obtained values in Table 2 that when the concentration increased, the value of corrosion rate decreased and the value of inhibition efficiency rose. The main reason for this is that the greater number of inhibitor molecules adsorbed on the metal surface and covered a large part of the metal surface.These findings are similar to previous research work [31]. Three inhibitors used in the present investigation, namely THA–H, THA–Br and THA–OCH$_3$, which have H, Br and OCH$_3$ substituents, respectively. All inhibitors show very high efficiency and the order of inhibition efficiency was found as follows: THA–Br < THA–H < THA–OCH$_3$. Among three inhibitors,THA–OCH$_3$exhibited the highest inhibition efficiency with 94.4% at 300 ppm and at 298K according to weight loss measurement. The reason for the superior inhibition nature of THA–OCH$_3$ is the methoxy group.This is due to the methoxy group is the good electron–donating group, and can easily donate the electrons to the empty d–orbitals of iron.

3.2. Adsorption mechanism

The adsorption isotherm is a very important tool to describe the adsorption process between the inhibitor molecule and the metal surface. In the present investigation, the Langmuir adsorption isotherm model fits were best to justify the adsorption. Usually, the Langmuir model expressed as given in Eq. 11 [32].

$$\frac{C}{\theta} = \frac{1}{K_{ads}} + C \tag{11}$$

Eq. 11 shows the correlationbetween the inhibitor concentration (C_{inh}) and the surface coverage (θ) on mild steel in 1M HCl at different concentrations. Slope and intercept were calculated from C_{inh}/θ vs C_{inh} plots.The graph of C_{inh}/θ vs C_{inh} (Fig 1) obtained at room temperature gives straight lines, revealing that Langmuir isotherm is the best fitting. The K_{ads} signifies resemblance among the adsorbate and adsorbent system. The higher values of K_{ads} for selected inhibitors indicates the good adsorption property of the molecule on the metal surface [5].The values of the adsorption
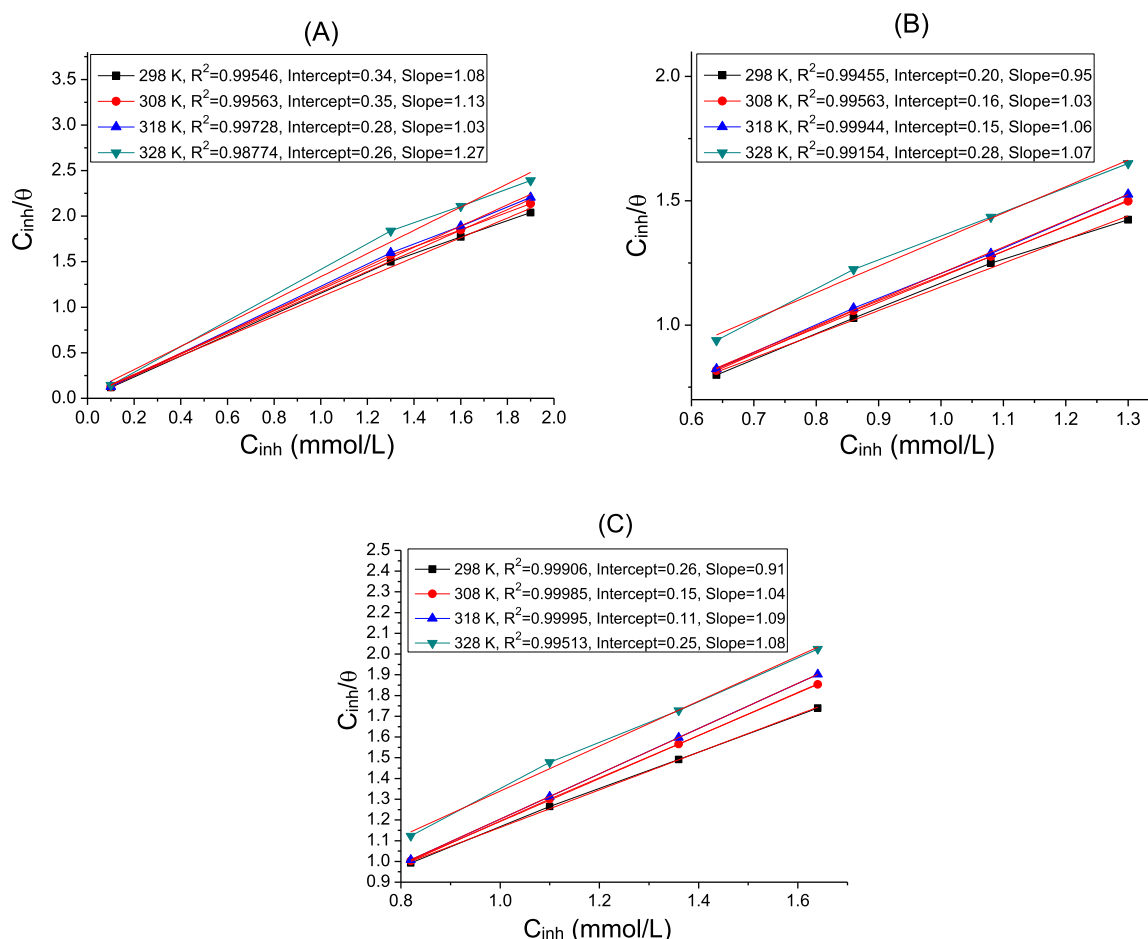
Fig. 1. Langmuir adsorption plots for studied inhibitors (a) THA-H, (b) THA-Br and, (c) THA-OCH$_3$ in 1M HCl solution at different temperatures.

constant (K_{ads}) were determined by the inverse value of the intercept (Fig. 1). Generally, the higher value of the adsorption constant showed that the adsorption efficiency of THA–H, THA–Br and THA–OCH$_3$ on the mild steel surface.It is also indicated that the selected inhibitors are more efficient at 298K– 328K ranges. Next, the values of K_{ads} and Gibbs free energy for adsorption (ΔG_{ads}) were calculated from Eq. 12 [32-34]:

$$\Delta G_{ads} = --2.303RTlog\left(55.5K_{ads}\right) \tag{12}$$

where R, T, and K_{ads} represent the gas constant, temperature at K, and absorption constant, respectively, 55.55 is the molar concentration of water at mol/L.

All the calculated data are summarized in Table 3. The negative value of G_{ads} shows the spontaneity of the absorption process of the inhibitor on the mild steel surface. A previous investigation suggests that a ΔG_{ads} less than -20 kJ/mol indicates that the adsorption mechanism is characterised by a physical nature; if it is more than -40 kJ/mol, adsorption occurs chemically [35-40]. In the present study, it was found that ΔG_{ads} values were –25.32, –264.78, and –24.72 kJ mol^{-1} for THA–H, THA–Br, and THA–OCH$_3$, respectively (Table 3), suggesting the studied inhibitors are mixed type. The negative value of G_{ads} (adsorption energy) shows that the studied inhibitors adsorb spontaneously on the metallic surface. In comparison to previous research works of [40-42], the studied inhibitors i.e. thiohydroxamic acid derivatives follow the physicochemical behaviour as their values are more than 20 kJ mol^{-1} and less than 40 kJ mol^{-1}.

Table 3
The values of G_{ads} and K_{ads} for the MS in the inhibitor absence and presence of 1 M HCl at various temperatures.

Inhibitor	Temp. (K)	R^2	K_{ads} (M^{-1})	ΔG_{ads} (kJ mol^{-1})
THA-H	298	0.998	340	-24.38
	308	0.998	350	-25.28
	318	0.998	280	-25.51
	328	0.997	260	-26.11
THA-Br			Average	**-25.32**
	298	0.999	200	-23.07
	308	0.998	260	-24.52
	318	0.997	250	-25.21
	328	0.998	280	-26.31
			Average	**-24.78**
THA-OCH$_3$	298	0.978	260	-23.72
	308	0.998	250	-24.42
	318	0.998	210	-24.75
	328	0.977	250	-26
			Average	**-24.72**

3.3. Electrochemical characterization

3.3.1. Potentiodynamic polarization(PDP) measurements

PDP analysis is applied to find out the adsorption property of THAs derivatives that is THA–H,THA–Br andTHA–OCH$_3$. Fig. 2 indicates the PDP plots for the inhibited system. Tafel indices such as the cathodic, anodic Tafel slopes (βc, βa), corrosion current densities (i_{corr}), and corrosion potential (E_{corr})were obtained from the PDP study (Table 4).Table 4 reveals that the increase in the con-
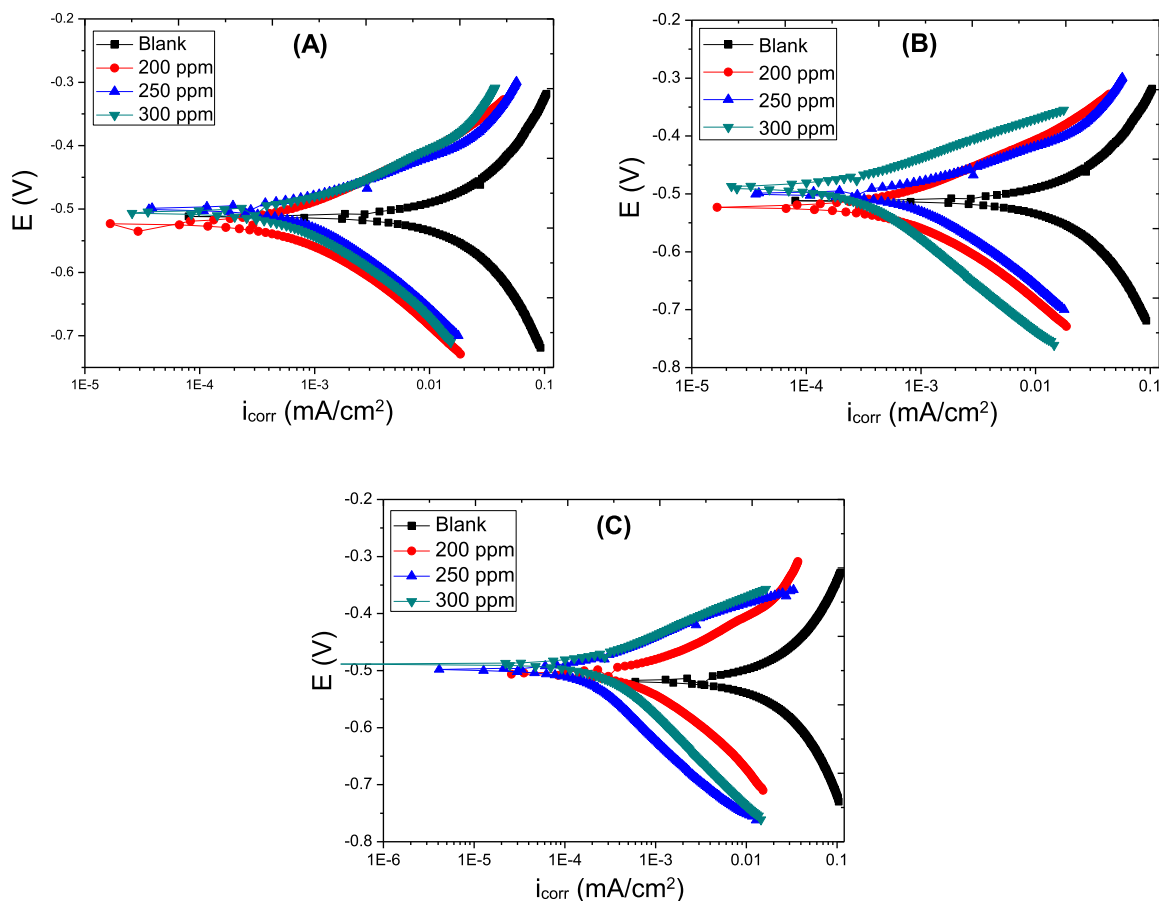
Fig. 2. Tafel plots for studied (a) MS/1M HCl/THA-OCH₃, (b) MS/1M HCl/THA-H and, (c) MS/1M HCl/THA-Br systems.

Table 4
Tafel polarisation parameters for THAs derivatives in 1 M HCl.

Inhibitors	Concentration (ppm)	Tafel polarisation parameters					
		i_{corr} $(A\ cm^{-1})$	$E_{corr\ (mV)}$	β_a $_{(mV\ dec^{-1})}$	β_c $_{(mV\ dec^{-1})}$	θ	$\%\eta$
THA-OCH₃	Blank	102.2	-513	270.2	304.8	–	–
	200	24.02	-504	218.16	285.31	0.764	76.49
	250	17.19	-499	215.32	278.65	0.831	83.18
	300	10.15	-518	206.41	269.41	0.900	90.06
THA-H							
	200	25.13	-524	131.1	222.3	0.754	75.41
	250	18.97	-513	145.2	131.9	0.814	81.43
	300	12.86	-510	113.9	162.2	0.874	87.41
THA-Br	200	25.87	-510	122.5	211.1	0.754	75.41
	250	19.64	-508	118.7	198.7	0.807	80.78
	300	13.45	-522	110.3	227.6	0.868	86.83

centration of inhibitors promotes the enhance in the value of corrosion current density, which indicates that the inhibitor molecules are deposited on the mild steel surface effectively and protect the steel surface from further corrosive attack. It is also indicated from observed data that the studied corrosion inhibitors formed the polarization block for the cathodic and anodic electrochemical reactions on the metal surface. The formation of a thin protective layer on the metal surface is mainly responsible for enhancing in the inhibition performance.Therefore, the presence of THAs molecules enhances the % η_{PDP}. The order of inhibition efficiencies measured by PDP analysis are in agreement with the results of the weight loss study; THA–Br < THA–H < THA–OCH₃.It was indicated related to the previous research articles [51-53] that if the value of E_{corr} between the inhibited and corrosive solution was greater than 85

mV, the inhibitor is usually anodic or cathodic. If E_{corr} value is less than 85 mV,the inhibition nature of the inhibitor is identified as amixed type inhibitor [43-45]. In this investigation work, E_{corr} value was less than 85 mV for the three THA derivatives, demonstrating that these inhibitors are the mixed type. The values of β_c and β_a given in Table 4 show that the values of β_c denote the cathodic property of the inhibitors more than the values of β_a. This mixed type is mainly due to the cathodic nature of inhibitors, revealing that the inhibitor molecules are predominantly adsorbing on the cathodic site of the mild steel surface.

3.3.2. Electrochemical impedance spectroscopy (EIS) measurements
    EIS measurement is a very effective tool to determine the adsorption and interfacial properties of inhibitor molecules [46]. EIS

Table 5
Impedance parameters for MS in 1 M HCl with and without THAs derivatives.

Inhibitor	Conc. (ppm)	R_s (Ω cm^{-2})	R_{ct} (Ω cm^{-2})	C_{dl} (μF cm^{-2})	θ	%η
THA-OCH$_3$	Blank	1.566	06.52	127.4	-	-
	200	1.013	25.43	90.53	0.744	74.36
	250	1.470	78.22	83.33	0.916	91.67
	300	1.988	120.4	66.31	0.950	95.08
THA-H	200	0.982	22.89	82.58	0.715	71.51
	250	1.503	73.51	76.65	0.911	91.13
	300	0.976	163.7	66.32	0.948	94.85
THA-Br	200	1.012	75.54	82.22	0.914	91.37
	250	0.969	122.4	75.31	0.937	93.67
	300	1.004	171.6	64.48	0.940	94.04
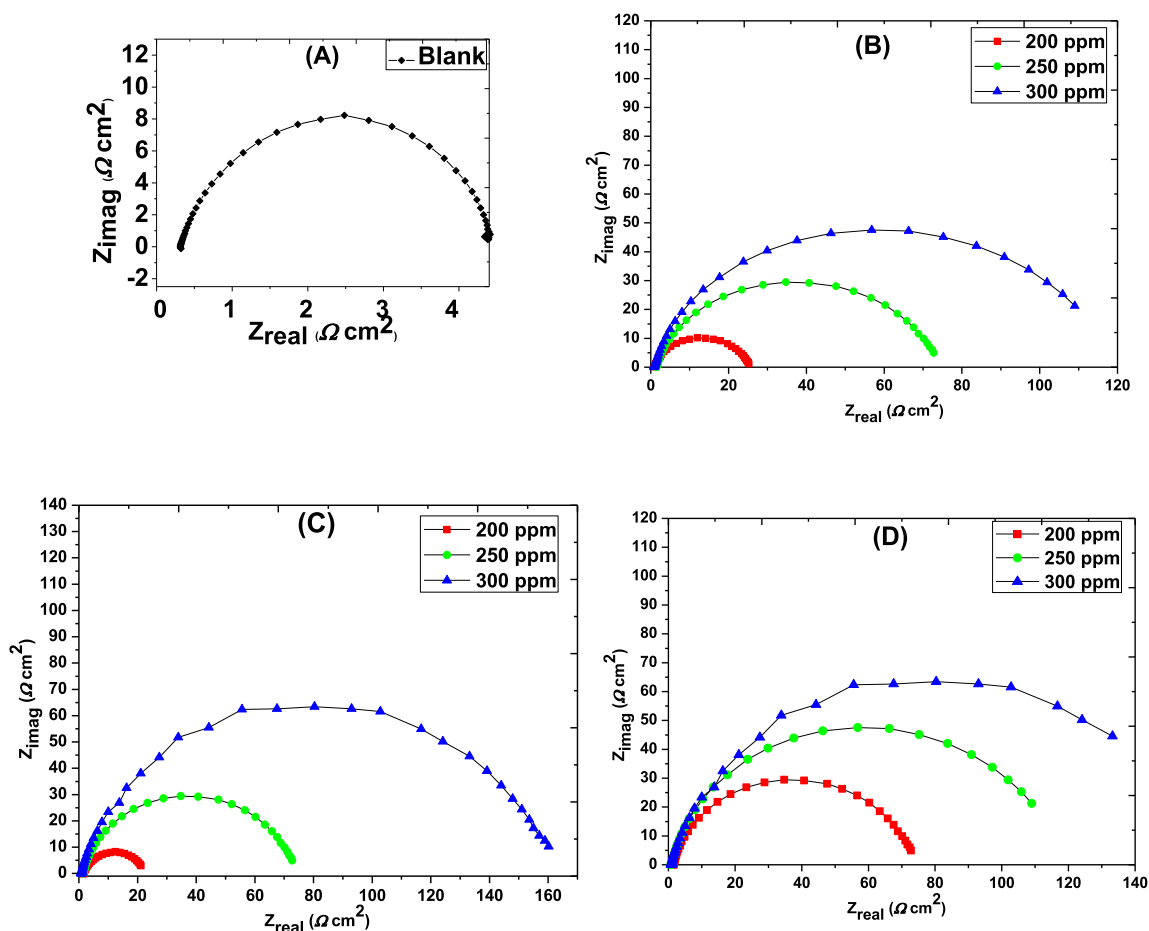
Fig. 3. Nyquist plot for studied (a) 1 M HCl (b) MS/1M HCl/THA-OCH$_3$, (c) MS/1M HCl/THA-H and, (d) MS/1M HCl/THA-Br systems.

wasapplied to characterize THA–H, THA–Br, and THA–OCH$_3$ inhibitors with different concentrations and temperatures ranging from 298–328 K. The R_s (solution resistance) R_{ct} (charge transfer resistance) and R_i (inductive resistance) have been calculated and the corresponding values are summarized in Table 5. The corresponding Nyquist plots obtained from EIS are represented in Fig. 3. The Nyquist plots are shown in Fig. 3 were depressed semicircle rather than a true semicircle, which is associated with inhomogeneity and roughness of the metal surface [47]. It is next stressed fact is that the Nyquist plots of the present study were one loop, which is a capacitive loop at higher frequencies, revealing the efficient adsorption characteristic of THAs derivative on the metal surface.In the equivalent circuit model, the double–layer capacitance (C_{dl}) was replaced by a constant phase element (CPE) to get a more precisely optimized fitting. The equivalent circuit fitting model is shown in Fig. 5. Eq. 13 represents the fitting of all experimental

data and can be represented as [48]:

$$Z_{CPE} = \left(\frac{1}{Y_0}\right)\left[(jw)^N\right]^{-1} \tag{13}$$

where,CPE represents capacitance, resistance, and impedance.

On the other hand, the value of C_{dl} was calculated for the corrosive and inhibited system. Eq. 14 indicates the double layer capacitance for the corrosion of MS in 1 M HCl. Double layer capacitance was estimated from the expression given in Eq. 14 [48]:

$$C_{dl} = Y_o (w_{max})^{n-1} \tag{14}$$

where,Y_o and n are the exponent and phase shift, respectively.

From Table 5, it is noted that the values of C_{dl} decreased gradually with the increase in the concentration, indicating the substitution of water molecules by the inhibitor molecule onthe metal–HCl interface. In the present work, the values of C_{dl} were found. Sim-
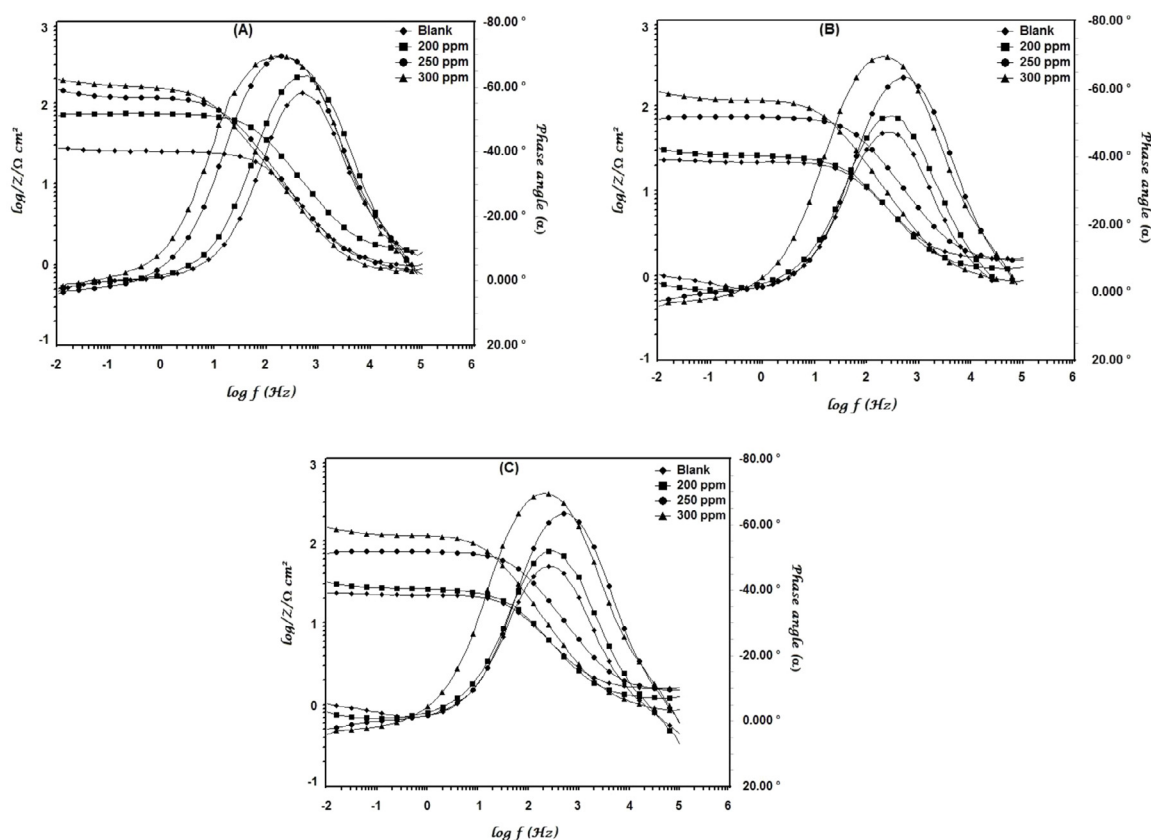
Fig. 4. Bode plots for studied (a) MS/1M HCl/THA-OCH₃, (b) MS/1M HCl/THA-H and, (c) MS/1M HCl/THA-Br systems.
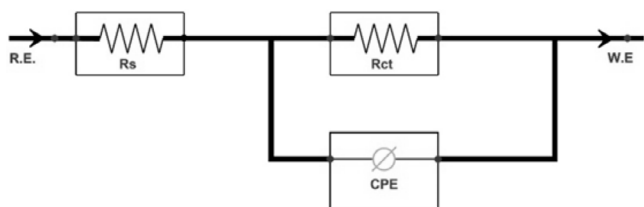

Fig. 5. Equivalent circuit model used for fitting the Nyquist curves

ilarly, Fig. 4 reveals the corresponding bode phase angle plots for THAs inhibitors. In the presence of THA derivatives, the phase angle value was greater than the value of 1M HCl solution (Fig. 4), which confirmed the following facts: the more negative phase angle value and the more capacitive behaviour support the increasing smoothness of mild steel surface with the presence of inhibitor. The above results suggested the efficient adsorption of inhibitors, decreasing the roughness of the metal surface [49,50]. Finally, the value of %η_{EIS} are were accounted for 94.85%, 94.04% and 95.08% for THA–H, THA–Br and THA–OCH₃, respectively, suggesting the good correlation with the observed data of weight loss experiment.

3.4. Surface characterization

3.4.1. SEM–EDS measurements

The SEM micrographs and EDS spectra of mild steel surface in the 1 M HCl without and with the inhibitors at optimum concentration are shown in Fig. 6 a–d and Fig. 7 a–c, respectively. Fig. 6 (a) exhibited the corrosion destruction on mild steel surface in the absence of inhibitors (1 M HCl), which may be due to the attack of corrosive chloride ion. Moreover, Fig. 6 (b–d) demonstrated the less pitch, clean, and plane surface, which may be due to the

presence of protective layers of inhibitor molecules deposited on the metal surface and formed a protective layer on the mild steel surface and protect from further corrosive attack [51]. The EDS results suggested the formation of protective film on the metal surface with the presence of inhibitor molecules [52].Values of elemental composition (wt %) corresponding to EDS spectra are summarized in Table 6. From Table 6, it can be seen that in the absence of inhibitors a higher concentration of chloride ion (6.11 wt %) reported. In comparison,the chloride concentration of 0.87%, 0.91%, and 1.23 % was found with the presence of THA–H, THA–Br and THA–OCH₃, respectively. These results revealed that the presence of high corrosive chloride ions on MS metal surface is responsible for corrosion. The amounts of chloride ions were importantly reduced by the presence of inhibitor molecules. Therefore, both SEM and EDS analyses confirmed the weight loss and electrochemical experiments.

3.4.2. XRD measurements

XRD is an advanced and prominent tool for the quantitative analysis, phase characterizations, and determination of the crystalline nature of materials. Before doing XRD analysis, the surface of the metal sample was cleaned. Fig. 8 represents the XRD pattern of metal samples obtained in 1 M HCl solution without and with inhibitor at the optimum concentration. It is stressed from the spectrum of Fig. 8a that the corrosion product included mainly oxide of iron accumulates on the metal surface in the corrosion solution. In the scratched sample with 1 M HCl, the peaks have appeared at $2\theta = 36.8°$, 53.2° and 53.5°, indicating the presence of iron metal oxide such as FeOOH. Fe₃O₄ on the metal sample while the value of spectra was $2\theta = 55.1°$ with the presence of THA–OCH₃ (300 ppm), showing the decrease in the percentage of iron oxyhydroxide (FeOOH) and ferric oxide (Fe₃O₄) [53]. From the above XRD analysis,it is suggested that the formation of iron oxide
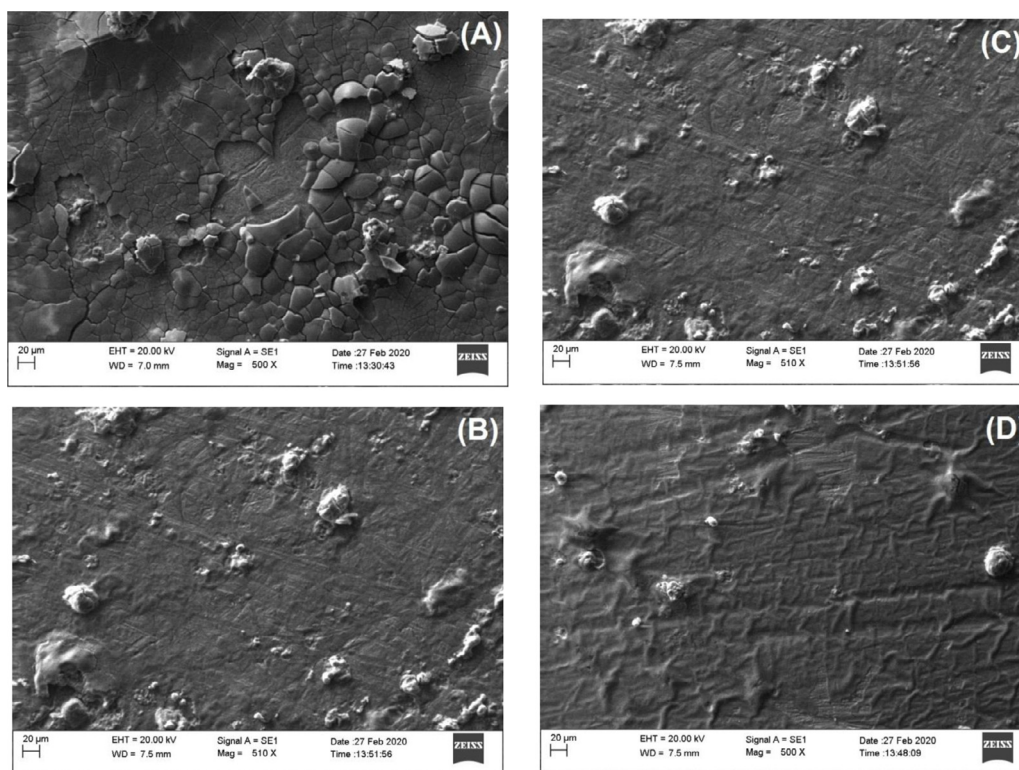
Fig. 6. SEM microphotographs for (a) MS/1M HCl, (b) MS/1M HCl/THA-H, (c) MS/1M HCl/THA-Br and, (d) MS/1M HCl/THA-OCH₃ systems.

Table 6
EDS parameters for THAs derivatives in 1 M HCl.

Medium	Composition (wt %)					
	Fe	Cl	O	S	C	N
MS/1M HCl system	92.58	6.11	0.84	0.31	0.16	-
MS/THA-OCH₃/1M HCl system	89.79	0.87	1.69	1.12	6.02	0.51
MS/THA-H/1M HCl system	90.41	0.91	2.71	0.97	4.52	0.48
MS/THA-Br/1M HCl system	90.74	1.23	2.54	0.92	4.13	0.44

on the metal surface was significantly blocked with the formation of protective film on the metal surface.

3.5. Quantum chemical calculations

To performthe density functional theory (DFT), the optimization structure, quantum chemical behaviour and reactivity of selected inhibitors can be successfully studied [54]. Important parameters such as the energy gap ($\triangle E$), frontier molecular energy (highest occupied molecular orbital (HOMO) and lowest unoccupied molecular orbital (LUMO)), global hardness, softness, electron fraction, electronegativity,etc.were calculated from the DFT calculation. All these parameters can explain the absolute properties of any inhibitors such as nucleophile nature, reactivity, adsorption nature [55].The frontier molecular orbitals can be used to explain the electron–donating and electron–accepting properties of a molecule.Typically, the lower the value of LUMO indicates the more inhibition effective, and the higher the value of HOMO is responsible for the good electron–donating property [56,57]. The values of energy corresponding to HOMO and LUMO are shown in Table 7. Fig. 9 (b, e & h) shows that the HOMO is more localized towards the electron–rich species in the THA–H, THA–Br, and THA–OCH₃, respectively.The electron density is more towards the p–electrons and unbounded electron containing atoms while LUMO is more localized towards the more electronegative atom (S and O), heteroatom-containing unsaturated carbonylbond and

lower electron density (Fig. Fig. 9 c, f & i) for THA–H, THA–Br, and THA–OCH₃,respectively.

It is underlined fact from the amountsof HOMO (Table 7) that the inhibition behaviour of THA–OCH₃ is higher than that of other thiohydroxamic acid derivatives. Experimental investigations also show that the inhibition performance of THA–OCH₃ is higher as compared to other derivatives. This is due to the presence of electron–donating methoxy substituent. Similarly, a low energy gap ($\triangle E$) between the LUMO and HOMO suggested the more reactive and adsorption property of inhibitor molecules. The following aspect is that the positive values of $\triangle N$ for all support that the electron flow from organic molecule to the metallic surfaceis easy and effective [27,31]. The electron transfer from the inhibitor molecules to the metal surface is also supported by the values of other parameters such as the electron fraction, global stiffness, softness, electromagnetism and dipole moments.

3.6. Fukui indices

The Fukui indices describe the most favourable sites for adsorption in the optimised structure of THA-H, THA–Br and THA–OCH₃ molecules. The values of local molecular reactive properties of THA–H, THA–Br and THA–OCH₃ were found and the obtained data are represented in Tables 9,10 and 11. The most nucleophilic (f_k^- high), electrophilic (f_k^+ high) and neutral (f_k^0 high) attacking sites in the THA–H, THA–Br and THA–OCH₃ molecules was
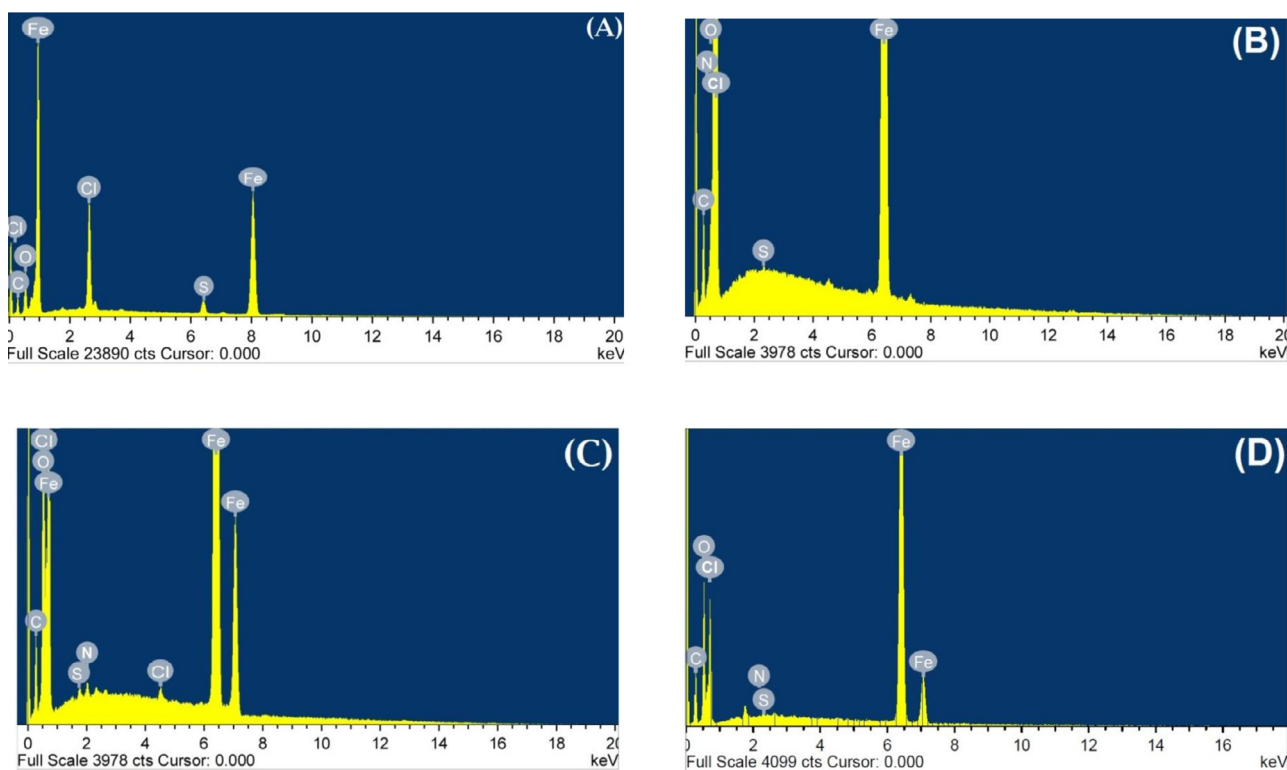
Fig. 7. EDS spectral images for (a) MS/1M HCl, (b) MS/1M HCl/THA-H, (c) MS/1M HCl/THA-Br and, (d) MS/1M HCl/THA-OCH$_3$ systems.

Table 7
DFT parameters of neutral forms of THAs derivatives

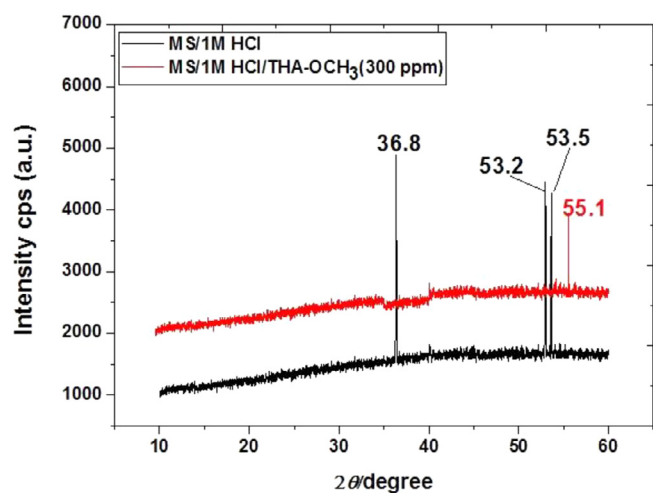| THAs	E_{HOMO} (eV)	E_{LUMO} (eV)	ΔE (eV)	IE	EA	η	χ	ω	σ	ΔN_{110}	μ (Debye)
THA-OCH$_3$	-5.99	-1.47	4.52	5.99	1.47	2.26	3.73	15.721577	0.44247788	0.24115044	3.6519
THA-H	-6.16	-1.66	4.5	6.16	1.66	2.25	3.91	17.1991125	0.44444444	0.20222222	3.6519
THA-Br	-6.32	-1.92	4.4	6.32	1.92	2.2	4.12	18.67184	0.45454545	0.15909091	3.6519

Fig. 8. XRD spectrafor (a) MS/1M HCl and, (b) MS/1M HCl/THA-OCH$_3$(300 ppm) systems.

measured through the Fukui function. In the Fukui analysis, the natural population analysis (NPA) was found and the resulted data were performed to derivate the Fukui indices (f_k^+, f_k^-, f_k^0) of the THA-H, THA-Br and THA-OCH$_3$ by Fukui functions, as indicated in Equations 15-17 [58]:

$$f_k^+ = P_k(N+1) - P_k(N) \tag{15}$$

$$f_k^- = P_k(N) - P_k(N-1) \tag{16}$$

$$f_k^0 = P_k(N+1) - P_k(N-1) \tag{17}$$

where $P_k(N+1)$, $P_k(N)$ and $P_k(N-1)$ are anionic, neutral and cationic molecules, respectively.

Table 9, 10 and 11 compared the most nucleophilic (f_k^- high), electrophilic (f_k^+ high) and neutral (f_k^0 high) attacking atoms in the THA-H, THA-Br and THA-OCH$_3$. It is clear from Table 9 that the 11C and 14S atoms are most nucleophilic; the 2C and 17C are most electrophilic; the 2C, 14S and 17C atoms are most neutral for THA-H. Table 10 indicates that the 10C and 13S are more nucleophilic; the 1C and 5C atoms are more electrophilic; the 1C, 5C and 13S are more neutral sites for THA-Br. It is noted in Table 11 that the 10C and 13S are more nucleophilic; the 4C and 5C atoms are more electrophilic; the 4C, 5C and 13S are more neutral attacking for THA-OCH$_3$. As concluded, the more nucleophilic and electrophilic attacking sites in the inhibitor molecules are attributed to the rise in the inhibition performance.

3.7. Molecular electrostatic potentials

The molecular electrostatic potentials (MEP) of the THA-H, THA-Br and THA-OCH$_3$were described in Fig. 10. MEP regions represented more reactive sites in the optimised structure of selected

Optimized Structure	HOMO	LUMO

(A) THA-H

a b c

(B) THA-Br

d e f

(C) THA-OCH₃

g h i
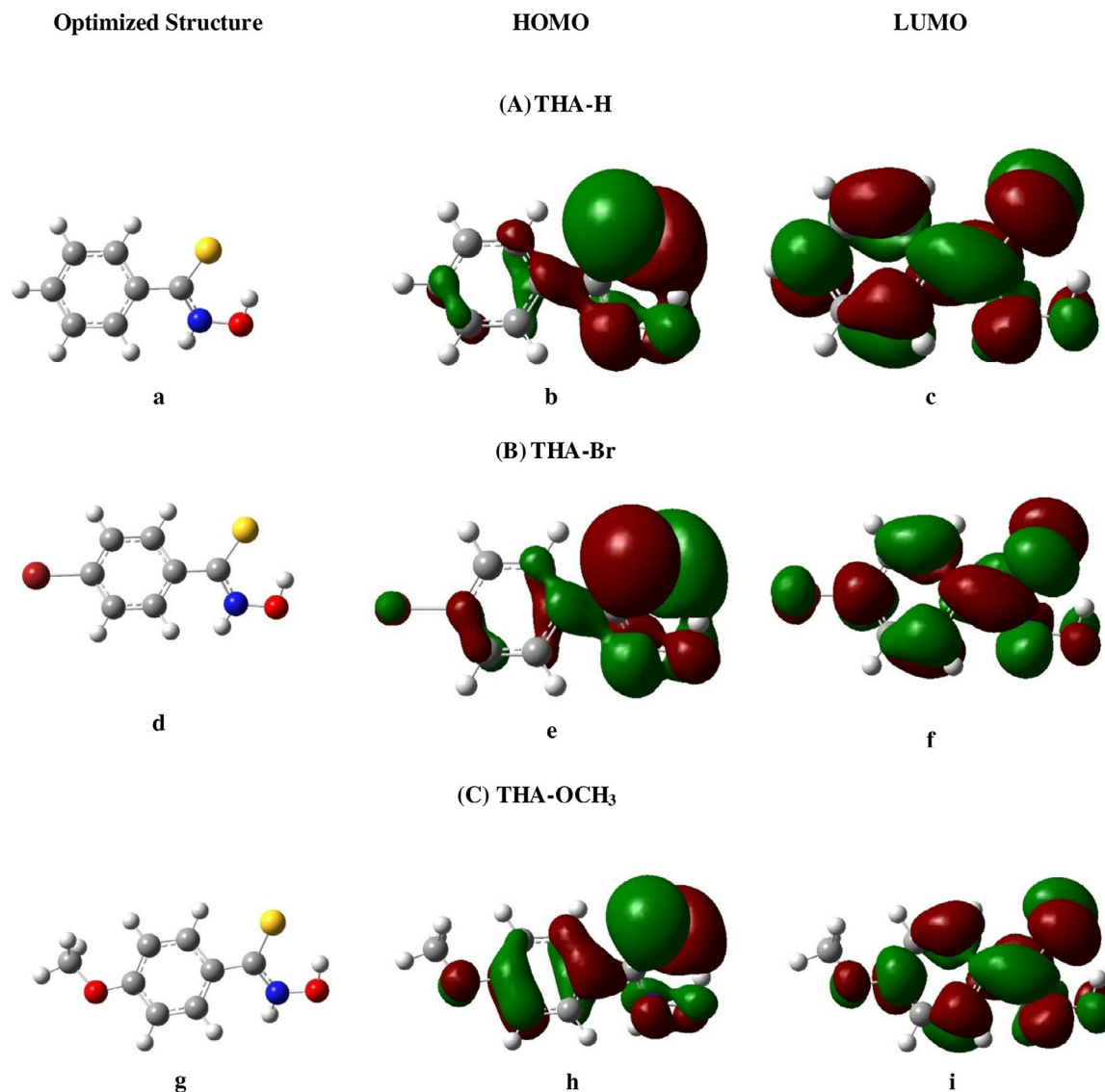
Fig. 9. The optimized structures (left), HOMO (middle) and LUMO (right) for thiohydroxamic acid derivatives (A) THA-H, (B) THA-Br, and (C) THA-OCH$_3$, respectively.
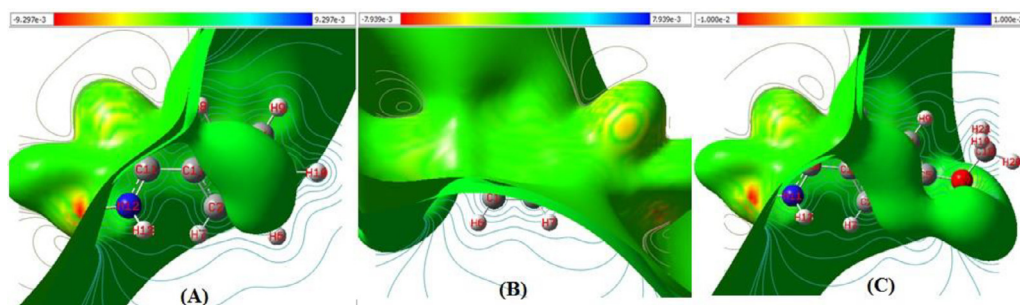
Fig. 10. Molecular electrostatic potential (MEP) of (A) THA-H, (B) THA-Br, and (C) THA-OCH$_3$, respectively.

inhibitor molecules. These most reactive regions indicated the nucleophilic and electrophilic attack positions in the optimised structure. In the resulted MEP, the red (negative) and blue (positive) regions revealed the nucleophilic and electrophilic reactivity positions in the THA–H, THA–Br and THA–OCH$_3$ molecules, respectively. It is also indicated that the obtained MEP of selected inhibitors were located at more negative regions, confirming that the

nitrogen, oxygen and sulfur atoms make inhibitor to become more effective.

3.8. Monte Carlo simulation

To deep understand the adsorption behaviour of the inhibitors on the metal surface, Monte Carlo simulations were performed on
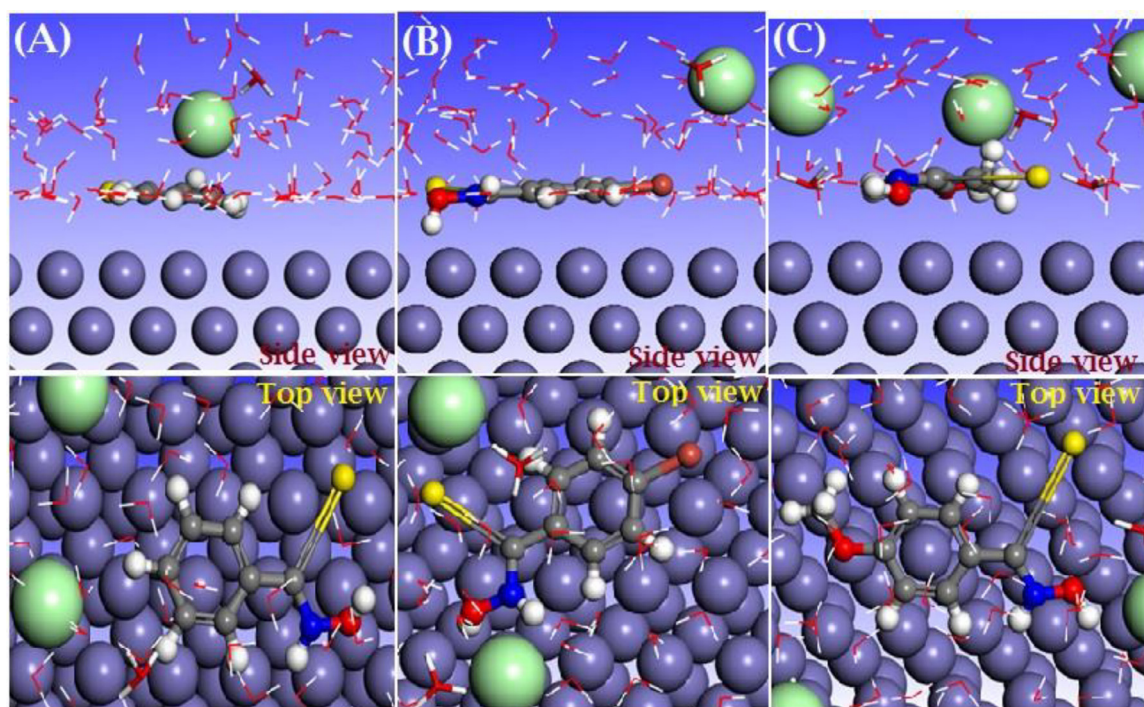
Fig. 11. The most stable low energy configuration (left side view & right top view) for the adsorption of studied molecules (a) THA-H, (b) THA-Br and (c) THA-OCH$_3$ on Fe (110) surface obtained using MC simulation.

Table 8
Adsorption energies for studied inhibitors on Fe(110)/ inhibitor system obtained using the Monte Carlo simulation (all units in kcal/mol).

System	E_{ads} (inh)	E_{ads} (H$_2$O)
Fe(110)/THA-OCH$_3$	-3599.70	-10.27
Fe(110)/THA-H	-3588.32	-12.75
Fe(110)/THA-Br	-3572.82	-13.76

Table 9
Fukui indices of THA-H.

№	Atom	f_k^-	f_k^+	f_k^0
1.	C	0.0002	0.0085	0.0043
2.	C	0.001	**0.4888**	**0.2449**
3.	C	0.0011	0.0076	0.0044
4.	C	0.0001	0.0009	0.0005
5.	C	0	0.0005	0.0003
6.	H	0	0	0
7.	H	0.0001	0.0001	0.0001
8.	H	0.0003	0	0.0001
9.	H	0	0	0
10.	H	0	0	0
11.	C	**0.0574**	0.0052	0.0313
12.	N	0.0055	0.001	0.0033
13.	H	0.0001	0	0.0001
14.	S	**0.9109**	0.0002	**0.4555**
15.	O	0.0007	0	0.0004
16.	H	0.0103	0	0.0051
17.	C	0.0122	**0.4872**	**0.2497**

Table 10
Fukui indices of THA-Br.

№	Atom	f_k^-	f_k^+	f_k^0
1.	C	0.0003	**0.5016**	**0.2509**
2.	C	0.0011	0.0078	0.0044
3.	C	0.0012	0.0002	0.0007
4.	C	0.0001	0.0081	0.0041
5.	C	0	**0.4795**	**0.2398**
6.	H	0	0	0
7.	H	0.0001	0	0
8.	H	0.0003	0	0.0001
9.	H	0	0	0
10.	C	**0.0577**	0.0004	0.029
11.	N	0.0057	0.0001	0.0029
12.	H	0.0001	0	0.0001
13.	S	**0.9107**	0	**0.4554**
14.	O	0.0007	0	0.0004
15.	H	0.01	0	0.005
16.	C	0.0121	0.0003	0.0062
17.	Br	0	0.002	0.001

Fe (110) surface taking into consideration the experimental conditions (the presence of the studied molecules in hydrochloric acid solution). The most stable low–energy adsorption forms of inhibitors on the Fe (110) / 200 H$_2$O molecule system are shown in Fig. 10. The adsorption energies for studied inhibitors on Fe (110)/ inhibitor systemare listed in Table 8. It could be seen from Fig. 11 that the investigated inhibitor molecules were preferentially oriented parallel on the Fe surface to maximize contact and in-

crease the surface coverage area. This adsorption model can be attributed to becoming the strong interaction between the phenyl rings of thiobenzohydroxamic acid and the metal surface. Moreover, these results also responsible for the strong interaction between the S, O atoms, several π–electrons and metal surface, which can offer the electron densities to the unoccupied–orbitals of iron to form coordinate bonds. Therefore, Monte Carlo simulations results confirmed the adsorption of the studied inhibitors and forming a stable barrier film on Fe (110) surface [59].The absolute value of the adsorption energies of the studied inhibitors on the simulated system follows the order: THA–OCH$_3$> THA–H > THA–Br. This order also supports by the experimental and DFT results. In all examined systems, the adsorption energies of selected inhibitors were far higher than that of water molecules. This observation reflects the possibility of gradual substitution of H$_2$O molecules with inhibitor molecules on the Fe (110) surface [30,31,60].
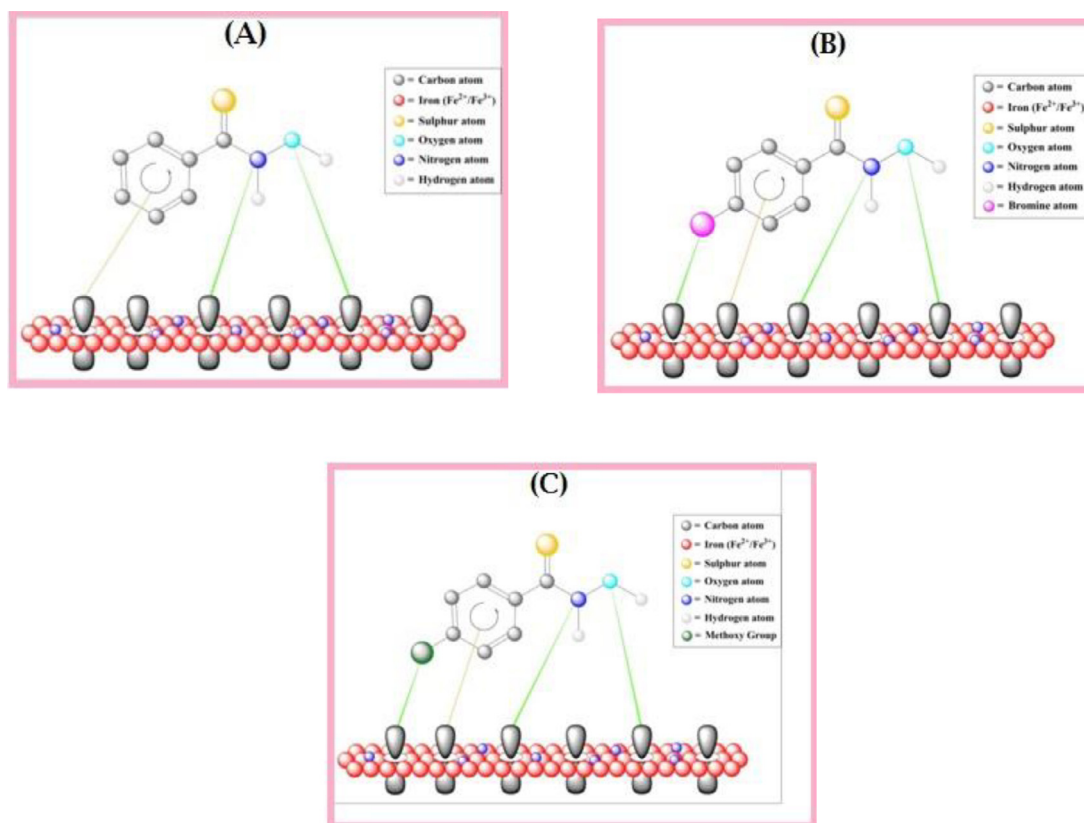
Fig. 12. Plausible adsorption modes of a) THA-H, b) THA-Br and, c)THA-OCH$_3$ molecules on MS surface.

Table 11
Fukui indices of THA-OCH$_3$.

№	Atom	f_k^-	f_k^+	f_k^0
1.	C	0.003	0.0075	0.0039
2.	C	0.0012	0.0002	0.0007
3.	C	0.0012	0.0073	0.0043
4.	C	0.0002	**0.4514**	**0.2258**
5.	C	0.0001	**0.5266**	**0.2633**
6.	H	0	0	0
7.	H	0.0001	0	0
8.	H	0.0003	0	0.0002
9.0	H	0	0	0
10.	C	**0.057**	0.0002	0.0286
11.	N	0.0056	0	0.0028
12.	H	0.0001	0	0
13.	S	**0.9104**	0	**0.4552**
14.	O	0.008	0	0.0004
15.	H	0.0107	0	0.0053
16.	C	0.012	0.0003	0.0062
17.	O	0	0.0064	0.0032
18.	C	0	0	0
19.	H	0	0	0
20.	H	0	0	0
21.	H	0	0	0

4. Adsorption mechanism

The adsorption energies of the THAs on the MS surface follows the order: THA–OCH$_3$> THA–H > THA–Br. This order is also supported by the result of weight loss and electrochemical analysis. Moreover, these results can be ascribed to the strong interaction between the metal surface and heteroatom's such S, O, N atoms and phenyl ring, which can offer electron densities to the unoccupied–orbitals of iron to form coordinate bonds. It is also indicated that the protective film was formed on the metal sur-

face with the presence of selected inhibitors [59,61].Fig. 12 (a–c) demonstrated the plausible adsorption mechanism of THA-H, THA–Br, and OCH$_3$. Usually, inhibitor molecules acted as a Lewis base. The electron-donating tendency of inhibitorson the metal surface behaves similar to a Lewis acid. This is due to the presence of vacant d orbitals of metal cations.It also stressed that the HOMO of inhibitor molecules and LUMO of metal cation interact with each other to form a stable bond [7,62,63].

5. Conclusion

The present investigation reveals the inhibition properties of THAs derivatives included N–hydroxybenzothioamide (THA–H), 4–bromo–N–hydroxybenzothioamide (THA–Br), and 4–methoxy–N–hydroxybenzothioamide (THA–OCH$_3$) towards corrosion of mild steel in 1 M HCl. The various experimental and computational techniques were performed for the determination of the inhibition nature of THAs derivatives. The following key points can be concluded from the present analysis:

1. The inhibition efficiencies of THA–OCH3, THA–H, and THA–Br was 94.26%, 93.21%, and 91.32%, respectively, according to WL analysis.
2. The presence of –OCH3 substituent group is responsible for higher inhibition efficiency of THA–OCH3 onthe mild steel surface.
3. PDP analysis confirmed the mixed type behaviours of all THAs.
4. The adsorption characteristics of all studied THAs were described as related to the Langmuir adsorption isotherm.
5. SEM–EDS surface analysis demonstrated that the protecting film on the MS surface was formed with the presence of an inhibitor.

6 XRD results confirmed that the presence of inhibitor importantly reduced the concentration of chloride ions from 6.11 wt% to around 1 wt%.

7 MD simulation exhibited that the adsorption energies of inhibitors are as follows:−3599.70kc al/mol for THA−OCH3, −3588.32 kcal/mol for THA−H and −3572.82 kcal/mol for THA−Br, respectively.

8 Theoretical calculations and experimental analysis showing good agreements in the present investigation.

Declaration of Competing Interest

The authors declare no conflict of interest

Acknowledgement

Supplementary materials

Supplementary material associated with this article can be found, in the online version, at doi:10.1016/j.molstruc.2021.130648.

References

[1] M. Yadav, et al., Corrosion inhibition effect of spiropyrimidinethiones on mild steel in 15% HCl solution: insight from electrochemical and quantum studies, RSC Adv. 5 (87) (2015) 70832–70848.

[2] R. Hsissou, et al., Development and potential performance of prepolymer in corrosion inhibition for carbon steel in 1.0 M HCl: outlooks from experimental and computational investigations, J. Colloid Interface Sci. (2020).

[3] A. Singh, et al., The effect of an N-heterocyclic compound on corrosion inhibition of J55 steel in sweet corrosive medium, N. J. Chem. 43 (16) (2019) 6303–6313.

[4] C. Verma, et al., Substituents effect on corrosion inhibition performance of organic compounds in aggressive ionic solutions: a review, J. Mol. Liq. 251 (2018) 100–118.

[5] N.J. Vickers, Animal communication: when i'm calling you, will you answer too? Curr. Biol. 27 (14) (2017) R713–R715.

[6] M. Yildiz, et al., Influence of 1-butyl-1-methylpiperidinium tetrafluoroborate on St37 steel dissolution behavior in HCl environment, Chem. Eng. Commun. 205 (4) (2018) 538–548.

[7] C. Lai, et al., Investigation on two compounds of O, O'-dithiophosphate derivatives as corrosion inhibitors for Q235 steel in hydrochloric acid solution, Open Chem. 15 (1) (2017) 263–271.

[8] X. Zuo, et al., Research of Lilium brownii leaves extract as a commendable and green inhibitor for X70 steel corrosion in hydrochloric acid, J. Mol. Liq. 321 (2021) 114914.

[9] B. Tan, et al., Corrosion inhibition of X65 steel in sulfuric acid by two food flavorants 2-isobutylthiazole and 1-(1, 3-Thiazol-2-yl) ethanone as the green environmental corrosion inhibitors: combination of experimental and theoretical researches, J. Colloid Interface Sci. 538 (2019) 519–529.

[10] R. Zhang, et al., The influence of grain size and grain orientation on sensitization in AA5083, Corrosion 72 (2) (2016) 160–168.

[11] J. Wang, et al., Investigation of some Porphyrin Derivatives as Inhibitors for Corrosion of N80 Steel at High Temperature and High Pressure in 3.5% NaCl solution containing carbon dioxide, Int. J. Electrochem. Sci. 13 (2018) 11961–11973.

[12] P.P. Kumari, P. Shetty, S.A. Rao, Electrochemical measurements for the corrosion inhibition of mild steel in 1 M hydrochloric acid by using an aromatic hydrazide derivative, Arab. J. Chem. 10 (5) (2017) 653–663.

[13] A.S. Reddy, M.S. Kumar, G.R. Reddy, A convenient method for the preparation of hydroxamic acids, Tetrahedron Lett. 41 (33) (2000) 6285–6288.

[14] J. Telegdi, T. Rigó, E. Kálmán, Molecular layers of hydroxamic acids in copper corrosion inhibition, J. Electroan. Chem. 582 (1–2) (2005) 191–201.

[15] J. Liu, et al., 1-Phenyl-1H-tetrazole-5-thiol as corrosion inhibitor for Q235 steel in 1 M HCl medium: combined experimental and theoretical researches, Int. J. Electrochem. Sci 15 (2020) 2499–2510.

[16] A. Singh, et al., Electrochemical and surface studies of some Porphines as corrosion inhibitor for J55 steel in sweet corrosion environment, Appl. Surf. Sci. 359 (2015) 331–339.

[17] S.-Y. Kwak, et al., Synthesis and dual biological effects of hydroxycinnamoyl phenylalanyl/prolyl hydroxamic acid derivatives as tyrosinase inhibitor and antioxidant, Bioorganic Med. Chem. Lett. 23 (4) (2013) 1136–1142.

[18] M.K. Gupta, et al., 2D-QSAR in hydroxamic acid derivatives as peptide deformylase inhibitors and antibacterial agents, Bioorg. Med. Chem. 10 (12) (2002) 3713–3716.

[19] P. Tkac, A. Paulenova, The effect of acetohydroxamic acid on extraction and speciation of plutonium, Separat. Sci. Technol. 43 (9–10) (2008) 2670–2683.

[20] E. Farkas, É.A. Enyedy, H. Csóka, A comparison between the chelating properties of some dihydroxamic acids, desferrioxamine B and acetohydroxamic acid, Polyhedron 18 (18) (1999) 2391–2398.

[21] D.K. Verma, et al., Experimental and computational studies on hydroxamic acids as environmental friendly chelating corrosion inhibitors for mild steel in aqueous acidic medium, J. Mol. Liq. 314 (2020) 113651.

[22] D.K. Verma, et al., Gravimetric, electrochemical surface and density functional theory study of acetohydroxamic and benzohydroxamic acids as corrosion inhibitors for copper in 1 M HCl, Result. Phys. 13 (2019) 102194.

[23] B.C. Lemercier, J.G. Pierce, Synthesis of thiohydroxamic acids and thiohydroximic acid derivatives, J. Organic Chem. 79 (5) (2014) 2321–2330.

[24] ASTMASTM G1-90 Standard Practice for Preparing, Cleaning, and Evaluating Corrosion Test Specimens, ASTM International West, Conshohocken, USA, 1999.

[25] D.K. Verma, F. Khan, Green approach to corrosion inhibition of mild steel in hydrochloric acid medium using extract of spirogyra algae, Green Chem. Lett. Rev. 9 (1) (2016) 52–60.

[26] C. Verma, M.A. Quraishi, Thermodynamic, electrochemical and surface studies of dendrimers as effective corrosion inhibitors for mild steel in 1 M HCl, Anal. Bioanal. Electrochem. 8 (2016) 104–123.

[27] V. Srivastava, et al., Amino acid based imidazolium zwitterions as novel and green corrosion inhibitors for mild steel: experimental, DFT and MD studies, J. Mol. Liq. 244 (2017) 340–352.

[28] A. Singh, et al., Effect of electron donating functional groups on corrosion inhibition of mild steel in hydrochloric acid: experimental and quantum chemical study, J. Taiwan Inst. Chem. Eng. 82 (2018) 233–251.

[29] I. Obot, N. Obi-Egbedi, Adsorption properties and inhibition of mild steel corrosion in sulphuric acid solution by ketoconazole: experimental and theoretical investigation, Corros. Sci. 52 (1) (2010) 198–204.

[30] S. Kaya, et al., Quantum chemical and molecular dynamic simulation studies for the prediction of inhibition efficiencies of some piperidine derivatives on the corrosion of iron, J. Taiwan Inst. Chem. Eng. 65 (2016) 522–529.

[31] Z. Salarvand, et al., Enhanced corrosion resistance of mild steel in 1 M HCl solution by trace amount of 2-phenyl-benzothiazole derivatives: experimental, quantum chemical calculations and molecular dynamics (MD) simulation studies, Corros. Sci. 114 (2017) 133–145.

[32] D.K. Verma, F. Khan, Corrosion inhibition of mild steel in hydrochloric acid using extract of glycine max leaves, Res. Chem. Intermediat. 42 (4) (2016) 3489–3506.

[33] B. Chugh, et al., Comparative investigation of corrosion-mitigating behavior of thiadiazole-derived bis-schiff bases for mild steel in acid medium: experimental, theoretical, and surface study, ACS Omega 5 (23) (2020) 13503–13520.

[34] M. Belghiti, et al., Computational simulation and statistical analysis on the relationship between corrosion inhibition efficiency and molecular structure of some hydrazine derivatives in phosphoric acid on mild steel surface, Appl. Surf. Sci. 491 (2019) 707–722.

[35] C. Verma, et al., 3-Amino alkylated indoles as corrosion inhibitors for mild steel in 1M HCl: experimental and theoretical studies, J. Mol. Liq. 219 (2016) 647–660.

[36] D. Verma, et al., Inhibition performance of Glycine max, Cuscuta reflexa and Spirogyra extracts for mild steel dissolution in acidic medium: density functional theory and experimental studies, Result. Phys. 10 (2018) 665–674.

[37] C. Verma, et al., 2, 4-Diamino-5-(phenylthio)-5 H-chromeno [2, 3-b] pyridine-3-carbonitriles as green and effective corrosion inhibitors: gravimetric, electrochemical, surface morphology and theoretical studies, RSC Adv., 6 (59) (2016) 53933–53948.

[38] E. Berdimurodov, et al., Inhibition properties of 4, 5-dihydroxy-4, 5-di-p–tolylimidazolidine-2-thione for use on carbon steel in an aggressive alkaline medium with chloride ions: thermodynamic, electrochemical, surface and theoretical analyses, J. Mol. Liq. (2020) 114813.

[39] E. Berdimurodov, et al., A gossypol derivative as an efficient corrosion inhibitor for St2 steel in 1 M HCl+ 1 M KCl: an experimental and theoretical investigation, J. Mol. Liq. (2021) 115475.

[40] B. Tan, et al., Insight into anti-corrosion nature of Betel leaves water extracts as the novel and eco-friendly inhibitors, J. Colloid Interface Sci. 585 (2021) 287–301.

[41] B. Tan, et al., Experimental and theoretical studies on the inhibition properties of three diphenyl disulfide derivatives on copper corrosion in acid medium, J. Mol. Liq. 298 (2020) 111975.

[42] B. Tan, et al., Papaya leaves extract as a novel eco-friendly corrosion inhibitor for Cu in H2SO4 medium, J. Colloid Interface Sci. 582 (2021) 918–931.

[43] C. Verma, et al., 5-Arylpyrimido-[4, 5-b] quinoline-diones as new and sustainable corrosion inhibitors for mild steel in 1 M HCl: a combined experimental and theoretical approach, RSC Adv. 6 (19) (2016) 15639–15654.

[44] C. Verma, M. Quraishi, A. Singh, A thermodynamical, electrochemical, theoretical and surface investigation of diheteroaryl thioethers as effective corrosion inhibitors for mild steel in 1 M HCl, J. Taiwan Inst. Chem. Eng. 58 (2016) 127–140.

[45] M. Yadav, et al., Corrosion inhibition performance of pyranopyrazole derivatives for mild steel in HCl solution: gravimetric, electrochemical and DFT studies, J. Mol. Liq. 216 (2016) 78–86.

[46] A. Singh, et al., Electrochemical, surface and quantum chemical studies of novel imidazole derivatives as corrosion inhibitors for J55 steel in sweet corrosive environment, J. Alloy. Compound. 712 (2017) 121–133.

[47] N. Odewunmi, S. Umoren, Z. Gasem, Utilization of watermelon rind extract as a green corrosion inhibitor for mild steel in acidic media, J. Ind. Eng. Chem. 21 (2015) 239–247.

[48] A. Singh, et al., Comprehensive investigation of steel corrosion inhibition at macro/micro level by ecofriendly green corrosion inhibitor in 15% HCl medium, J. Colloid Interface Sci. 560 (2020) 225–236.

[49] M. Yadav, T. Sarkar, I. Obot, Carbohydrate compounds as green corrosion inhibitors: electrochemical, XPS, DFT and molecular dynamics simulation studies, RSC Adv., 6 (111) (2016) 110053–110069.

[50] R. Aslam, et al., N, N′-Dialkylcystine Gemini and Monomeric N-Alkyl Cysteine Surfactants as Corrosion inhibitors on mild steel corrosion in 1 M HCl solution: a Comparative study, ACS Omega 2 (9) (2017) 5691–5707.

[51] W. Zhang, et al., 9-Substituted acridines as effective corrosion inhibitors for mild steel: electrochemical, surface morphology, and computational studies, N. J. Chem. 44 (16) (2020) 6464–6474.

[52] M. Quraishi, R. Sardar, Corrosion inhibition of mild steel in acid solutions by some aromatic oxadiazoles, Mater. Chem. Phys. 78 (2) (2003) 425–431.

[53] P. Muthukrishnan, et al., Inhibition of the corrosion of mild steel in acidic media by use of a new antipyridine derivative, Res. Chem. Intermediat. 41 (9) (2015) 5961–5984.

[54] A.M. El Defrawy, M. Abdallah, J.H. Al-Fahemi, Electrochemical and theoretical investigation for some pyrazolone derivatives as inhibitors for the corrosion of C-steel in 0.5 M hydrochloric acid, J. Mol. Liq. 288 (2019) 110994.

[55] I. Abdulazeez, et al., New imidazole-based dimers as potential inhibitors for mild steel corrosion in acidic media: electrochemical and DFT evaluation, Mater. Corros. 71 (2) (2020) 292–299.

[56] K. Ansari, et al., Corrosion inhibition of N80 steel in 15% HCl by pyrazolone derivatives: electrochemical, surface and quantum chemical studies, RSC Adv., 6 (29) (2016) 24130–24141.

[57] K. Zhang, et al., Halogen-substituted imidazoline derivatives as corrosion inhibitors for mild steel in hydrochloric acid solution, Corrosion Sci. 90 (2015) 284–295.

[58] E. Berdimurodov, et al., Thioglycoluril derivative as a new and effective corrosion inhibitor for low carbon steel in a 1 M HCl medium: experimental and theoretical investigation, J. Mol. Struct. 1234 (2021) 130165.

[59] I. Obot, et al., Experimental, quantum chemical calculations, and molecular dynamic simulations insight into the corrosion inhibition properties of 2-(6-methylpyridin-2-yl) oxazolo [5, 4-f][1, 10] phenanthroline on mild steel, Res. Chem. Intermediates 39 (5) (2013) 1927–1948.

[60] D.K. Verma, et al., Investigations on some coumarin based corrosion inhibitors for mild steel in aqueous acidic medium: electrochemical, surface morphological, density functional theory and Monte Carlo simulation approach, J. Mol. Liq. (2021) 115531.

[61] E. Berdimurodov, et al., New anti-corrosion inhibitor (3ar, 6ar)-3a, 6a-di–p–tolyltetrahydroimidazo [4, 5-d] imidazole-2, 5 (1 h, 3h)-dithione for carbon steel in 1 M HCl medium: gravimetric, electrochemical, surface and quantum chemical analyses, Arab. J. Chem. 13 (10) (2020) 7504–7523.

[62] W. Zhang, et al., Halogen-substituted acridines as highly effective corrosion inhibitors for mild steel in acid medium, J. Phys. Chem. C 122 (44) (2018) 25349–25364.

[63] E. Berdimurodov, A. Kholikov, K. Akbarov, L. Guo, Experimental and theoretical assessment of new and eco–friendly thioglycoluril derivative as an effective corrosion inhibitor of St2 steel in the aggressive hydrochloric acid with sulfate ions, J. Mol. Liq. (2021), doi:10.1016/j.molliq.2021.116168.